Bulgarian Academy of Sciences. Space Research and Technology Institute.
Aerospace Research in Bulgaria. 38, 2026, Sofia

DOI: https://doi.org/10.3897/arb.v38.e04

QUASI-PERIODS IN THE LIGHT CURVE OF THE LBV STAR AF ANDROMEDAE REVEALED BY THE SEF METHOD

Tsvetan Georgiev, Petko Nedialkov

Sofia University "St. Kliment Ohridski", Department of Astronomy, Faculty of Physics
e-mail: tsgeorg@astro.bas.bg; japet@phys.uni-sofia.bg

Key words: *Time series: Periods; LBV stars; AF And*

Abstract

We analyse the B-band historical light curve of AF And (1918–19901) using our Structure Eminence Function (SEF) method. It extracts and characterises repetitive structures (patterns) responsible for quasi-periods (QPs) in time series. SEF is the dependence of structural eminence on the structure length. The positions of the SEF peaks indicate QPs. An advantage of the SEF method is its ability to represent the QP profile (the shape of the repetitive structure). The skewness of the profile may hint at the QP's nature, e.g., "obscure" or "flash". In this study, we describe and apply 4 variants of the SEF method. We emphasise 2 QPs at 3.90 and 4.55 yr (± 0.05 yr). The profile of QP at 4.55 yr poses positive skewness. Compared to Eta Car, where in our recent work we found two QPs, the SEF humps of AF And are about 1.5 times less prominent. For the present, we are unable to associate some of these QPs with the established periodic phenomenon of AF And. However, the similarity between pairs of QPS of Eta Car and AF And hints at the possible binarity of AF And.

Introduction

Recently, we analysed B- and V-band light curves (LCs) of the Galactic LBV Eta Carinae over the time interval 1823–2023 (Georgiev et al. 2025, G+25). Using our Structure Eminence Function (SEF) (Georgiev 2023, G23), we found two photometric quasi-periods (QPs). We also applied the periodogram methods CLEAN and Lomb-Scargle in a comparative framework. The well-prominent QP of 5.6–5.7 yr can be linked to the established orbital period of 5.54 yr. While the mass loss rate of this system is about 10^{-3} $M_\odot$ yr^{-1}, such a notable increase in the orbital period over a century may be real. The less prominent QP of 4.9 yr may be explained somewhat with emissivity in the optical that originates in a large volume (G+25).

The LBV AF And belongs to the most luminous stars in M31. The mass of such a star is 50–120 $M_\odot$. Probably because of its dense stellar wind, its peculiar emission line spectrum is very similar to the spectrum of Eta Car. In the last century, AF And shows complicated variability in the B-band interval of 15.5–17.6 mag, as well as more than 10 outbursts. In the quiescent state, the absolute magnitude is about – 8.2 mag and the spectral class is Of or WR (Humphreys et al. 2014). Then the temperature is about 33 000 K and the mass loss rate is about 2.2 × 10^{-4} $M_{\odot}$ yr^{-1} (Joshi 2019). During an outburst, the luminosity becomes about 10^5 $L_{\odot}$. Gallagher et al. (1981) maintained that "the evolution of a massive star to its core helium-burning phase at AF And's position in an interarm region of M31 supports a binary interpretation". The radius of AF And as a single star is estimated to be 63 $R_{\odot}$ (Szeifert et al. 1996).

Earlier, we began testing our SEF method on the historical LC of AF And (Georgiev et al. 2024, G+24). In this paper, we continue describing and applying the method. This text contains: 1. SEF method and its 4 variants; 2. QPs in the LC of AF And; 3. SEF profiles of QP structures; 4. Supplementary illustrations; 5. Summary. The abbreviations used are as follows:

AV – average value;	QP – quasi-period;
BP – beat period;	RLC – residual LC;
dp – data point number;	SD – standard deviation;
LC – light curve;	SEF – structure eminence function;
PE – power exponent;	TS – time step;
PGF – periodfgraph function;	WS – window size of smoothing.

1. The SEF method in 4 variants

The SEF method (Fig. 1) reveals and characterises repetitive structures (patterns) responsible for LC QPs. SEF is a dependence of the eminence (amplitude) of the structure on the length of time of the structure. Any prominent repetitive structure causes the maximum SEF “SEF build”). Further, our Periodograph Function (PGF), a "derivative" of SEF, shows clearly the SEF structure. The PGF is an SEF after subtraction of the SEF background and normalization to this background (see “PGF build”). The PGF humps are a spectrum of the QPs, like the results of other periodogram methods.

Preparatory procedures ensure a dense and flat input LC for the SEF build (if needed). Aiming for dense enough LC, we may perform resampling of the original LC by linear interpolation with a suitable constant time step (TS) (Figs. 2a, 3a, 5a, 7a). The resampling procedure omits local noise peaks and produces a somewhat smoothed LC. We may also perform the completion of the original LC, adding interpolated data in the large LC gaps (Figs. 2b, 4a, 6a, 8a). This procedure keeps the noise peaks. The output of the resampling or completing procedure is the input LC for the detrending procedure (Fig. 1).

The SEF method requires ***flat (detrend) LC***, i.e. LC with zero average value (AV). We may perform **local detrend** (removal of short-scale trend). The code smooths the LC "point-by-point" with a moving average. The code extracts the smoothed LC from the input LC and derives residual LC (RLC) (Figs. 3b–6b).

The smoothing window size (WS) is chosen to ensure good protrusion of the humps in the initial part of the PGF (see also Fig. 12). We may also perform **global detrend** (removal of long-scale trend). The code fits the LC by a low-degree polynomial, extracts the fit from the LC, and derives RLC (Figs. 7a, 8a). The RLC is characterised by zero AV and some standard deviation (SD). After local or global detrend, the result RLC is a flattened version of the LC, which is the input LC for SEF build (Fig. 1, Figs. 3c–8c).

SEF build is based on extracting and averaging RLC segments with length $L = L_{nin} \dots L_m$ and deriving their signal and noise profiles. The relevant SEF value is $E_L = A_I/D_L$, where A_L and D_L are suitable AV and SD characteristics of the signal and noise profiles.

Let's (t_i, z_i), $I = 1 \dots N$ be a ***uniformly sampled RLC,*** dense and flat, with TS δt, zero AV, and relevant SD. For SEF^I, build our code to search for repetitive structures, checking RLC segments with length L data points (dp) or time length (QP) tL = (L – 1) × δt, between Lmin and L_{max}, as follows. For every current L, the code pulls up the first L RLC data z_i, I = 1 ... L, and puts them into an initially empty 1D set x_j with cell numbers $j = 1 \dots L$. Then, it adds over there the next L data z_i, $I = L + 1 \dots L + L$ from the RLC. Later, it adds the next L data, etc. The (integer) number of possible additions is $k = N/L$. In the end, for the current L, every cell x_j contains k adds and has relevant AVs a_j and SDs d_j. Further, the code continues with the next segment length L, etc. So, each structure with length L dp is described by signal profile a_j and noise profile d_j (see also Fig. 10a). For the SEFs in Figs. 3c–8c, we specify L_{min} = 20 dp or t_{min} = 1 yr with TS δt = 0.05 yr. For statistical significance of signal and noise profiles, we need at least $k = 3$ additions of segments for every L. Therefore, the code extracts and adds segments of maximum length $L = N/3$ dp. For example, the RLC in Fig. 5b has N = 932 dp. So, in Fig. 5c we use L_{max} = 310 dp or t_{max} = 15.5 yr. There, the segment with length 20 dp (1 yr) contains k = 932/20 = 46 additions.

Now, let (t_i, z), $i = 1 \dots N$ be an ***arbitrary sampled RLC,*** dense and flat, with zero AV and relevant SD. In the previous case, we used a 1D set x_j with L cells to accumulate uniformly sampled RLS segments. Now, a 2D area (x_j, y_j) with N cells is necessary for collecting arbitrary sampled RC segments with their values and times. The code checks the system of time segments $t_l = t_{min} \dots t_{max}$ with a step of increasing δt. Similarly to the previous case, we supply t_{min} = 1 yr and δt = 0.05 yr. Again, for at least $k = 3$ additions, the code uses $t_{max} = t_{RLC}/3$. For the extraction of segments, the code derives the left bounds of the k-th positions of the current segment with length t_L in the RLC, $b_k = t_{min} + (k - 1)\,\delta t$. Then, for every t_L, the code pulls up the available n_1 RLC data starting with the time length t_L and places them in an empty 2D set at $x_i = t_i - b_1$, $y_i = z_i$, $i = 1 \dots n_1$, with cell numbers $j = 1 \dots n_1$. After that, it transfers the next n_2 data from the second RLC position of the segment to the 2D area: $x_{n1} + I = t_i - b_2$, $y_i = z_i$, $i = n_1 \dots n_1 + n_2$, etc. For every t_L, the data in the 2D area has to be sorted by time $x$thtt. The sorted data covers a segment with length t_L, and there is a "raw profile" of the structure with length $t_{L.}$ Later, the raw profile is smoothed by a moving average with TS 0.1 yr and WS 0.4 yr. (Applying TS of 0.05 yr and WS 0.2 yr is not applicable here because of the low density of the available completed RLC). The result is the signal profile a_j and the noise profile d_j. Further, the code checks the next segment, with length t_{L+1}, etc. As in the case with resampling, every structure with time length t_L is described by a signal profile a_j and a noise profile d_j (see also Figs. 10b, 10c).

Later, in both RLC cases, for every L or t_L, the code derives average signal $A_L = < |a_j| >_L$ and average noise $D_L = <d_j>_L$. Note that A_L gathers absolute values $|a_j|$, i. e. A_L is a one-sided average signal of the structure. Every prominent repetitive structure in the RLC produces a local maximum in the signal function A and a local minimum in the noise function D (G23). Therefore, we ought to define the **dimensionless SEF** (Figs. 3c–8c) as follows: $E_L = A_L/D_L$ or $E(t) = \mathrm{A}(_t)/D(t)$. In this study, the division by D "increases" the signal by about 3.8 times (Fig. 9a).

PGF build is a transformation of the SEF by background removal, aiming to better reveal the QPs. We consider the SEF background to be the curve that encloses 90% of the SEF data points from below. Generally, the SEF fit E_F (Figs. 3c–8c, dashed curves) is a power function and a linear function on the log-log scale. Therefore, the background is easily derived by shifting the relevant SEF straight line downward. Later, after transformation back into the linear scale, the SEF background straight line becomes a power function E_B (Figs. 3–8c, solid curves), with the same power exponent. So, we define the **dimensionless PGF** using the SEF values E and SEF background E_B as follows: $G_L = (E–E_B)/E_B$ or $G(t) = (E(t) – E(t)_B)/E(t)_B$. The PGF value characterises the relative height of the SEF value above the SEF background. Each PGF value represents a form of signal-to-noise ratio.

Basic QP p may be suspected among QPs by (i) a high peak in the initial part of the PGF and (ii) the presence of its large counterparts 2p, 3p, etc. But, in this study, we find 3 prominent QPs (Figs. 3c–8c, 3d–8d). In Figs. 3c, 4c large counterparts are visible up to 8p. In the cases of RLC with high resolution and low noise, short counterparts p/2, p/3, etc. may be seen (in G23 – up to p/7). The protruding of default short counterparts is especially modelled in G23. Furthermore, (iii) the profile (shape) a_j of the basic QP is single, i.e., it contains one minimum and one maximum. Such are also the profiles of $p/2$, etc., but they are faint (G23). However, the profiles of the large counterparts are double, triple, etc. (G23, G+25; bottom panels in Figs. 3–8). Finally, (iv) the basic QP may be recognised as a real period if its physical reason is clear. Unfortunately, in this study, we don't have such a true period.

Note that in the SEF build, the number of segment additions k is an integer and a part of the RLC, near its end, becomes unusable. To suppress this effect, we build SEF, QP profiles, and PGF twice, by direct and reverse processes of the RLC. The average profiles and PGFs results are always regarded (Fig. 11).

Fig. 1 presents a schematic overview of 4 variants (v1–v4) of the SEF method. The variants are arranged in vertical succession, as follows.

v1 includes (i) resampling of the original LC with a constant time step, (ii) local detrending by moving AV with a suitable WS, and (iii) SEF^{I} build.

v2 includes (i) filling the gaps in the original LC to achieve suitable data density, (ii) local detrending as in V1, and (iii) SEF^{II} build.

v3 includes (i) resampling as in v1, (ii) global detrend by smoothing the resampled LC using a low-degree polynomial, and (iii) SEF^{I} build.

v4 includes (i) filling the gaps as in v2, (ii) global detrending of the completed LC as in v3, and (iii) SEF^{II} build.

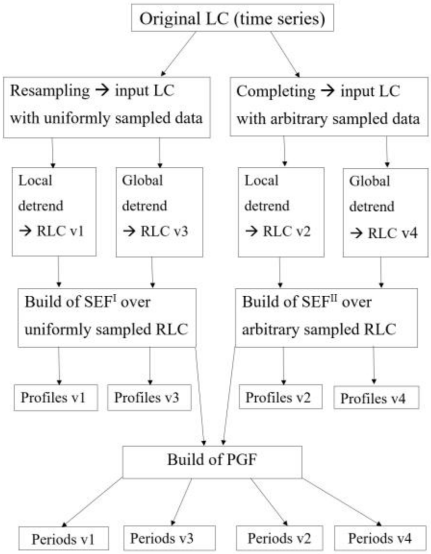

Fig. 1. Scheme of the procedures in the SEF 4 versions. See the text.

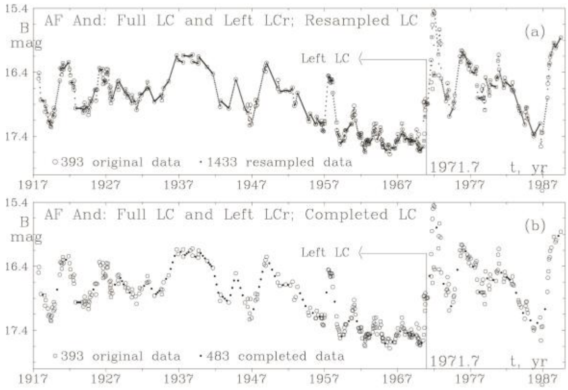

Fig. 2. Historical LC of AF And with resampled (a) or completed (b) version. See the text.

2. QPs in the LC of AF And

Fig. 2 shows the *B*-band LC (1917.7–1989.4; 71.7 yr), collected by Gantchev et al. (2017). The original LC (circles) contains 393 dp with an AV TS of 0.183 yr and a maximal data gap of 1.52 yr. In Fig. 2a, the original LC is resampled by linear interpolation with a TS of 0.05 yr. The result LC contains 1433 dp (dots only). In Fig. 2b, large gaps in the original LC are filled with interpolated data. The result LC contains 483 dp (circles and dots). The AV TS is 0.15 yr, and the maximal gap width is 0.4 yr. Further, the "Full LC" is analysed in Fig. 3, Fig. 4, while the "Left LC", 54 yr long, before the eruptions in 1971–1973, is analysed in Figs. 5–8. The rRight part of the full LC is too short for separate SEF analysis.

Figs. 3a–8a show by dots (1) the input LCs, resampled or completed from the original LC. Their parameters are time episode *T*, number of data *N*, AV and SD in magnitudes, as well as TS or average TS (<TS>). The dashed lines show the levels of AV and AV ± SD. The dots of the curves (2) are the smoothed input LC according to the applied SEF variant, v1–v4.

Figs. 3b–8b show the RLC, derived as the difference between the input LC and its smoothed version. Note that for convenience, when the brightness increases, the RLC value must also increase. Therefore, working with input and smoothed LCs in magnitudes, B_I and B_S, respectively, we use everywhere the RLC with opposite sign: $\Delta B(t) = -[B_I(t) - B_S(t)]$. The RLC parameters, as in panel (a), are *N*, SD, and time episode. The dashed lines show the zero level and zero ± SD. In Figs. 3b–6b, the local smoothing WS is shown by a bar. The choice of WS of 6.45 yr or 129 dp is illustrated in Fig. 12. Due to the local smoothing, the edges of the input LC, each of length WS/2, are lost, and the episode is shorter. In Figs. 7b, 8b, after global smoothing (by a second-degree polynomial), the entire length of the input LC is used. Due to the smoothing effect of resampling, the SD of the RLC (Figs. 3b, 5b, 7b) is about 0.03 mag lower than that of the completed RLC (Figs. 4b, 6b, 8b).

Figs. 3c–8c show SEF^{I} derived from uniformly sampled RLC (Figs. 3c, 5c, 7c) or SEF^{II} derived from arbitrarily sampled RLC (Figs. 4c, 6c, 8c). The curves E_F and E_B represent the power fit models of the SEF and SEF background. Power exponent (PE) is implemented. The suspected exemplary basic QP is p = 3.9 yr. Its large counterparts, 2p, 3p, etc., are visible up to 8p in Figs. 3c, 4c, and. up to 4p in Figs. 5c–8c. The SEFs begin from $\{t_{min}$ = 1 yr or $L_{min}\}$ = 20 dp and ends at $t_{max} = t_{RLC}/k$, where k is the number of the segment added to the AV profile; here, k_{min} = 3. In Figs. 5c, 6c, the SEF length is 15.5 yr, and in Figs. 7c, 8c, it is 17.5 yr, respectively. Especially in Figs. 3c, 4c, for k_{min} = 2, the SEF t_{max} is 27.5 yr. The reason is searching for beat periods (see below). The SEF increase F is due to covering stronger LC variations. The PEs' values, 0.8–1.0, show that here the SEFs are slightly convex.

Figs. 3d–8d show the initial parts of the PGFs *G*(t), derived from the relevant SEFs. The hump resolution of the SEF method may be estimated by the half-width at half of the hump maximum. Here, for a QP of 3.9 yr, it is about 4 dp or 0.2 yr. The relative hump resolution is about 5% of the QP value, as in G+24 and G+25.

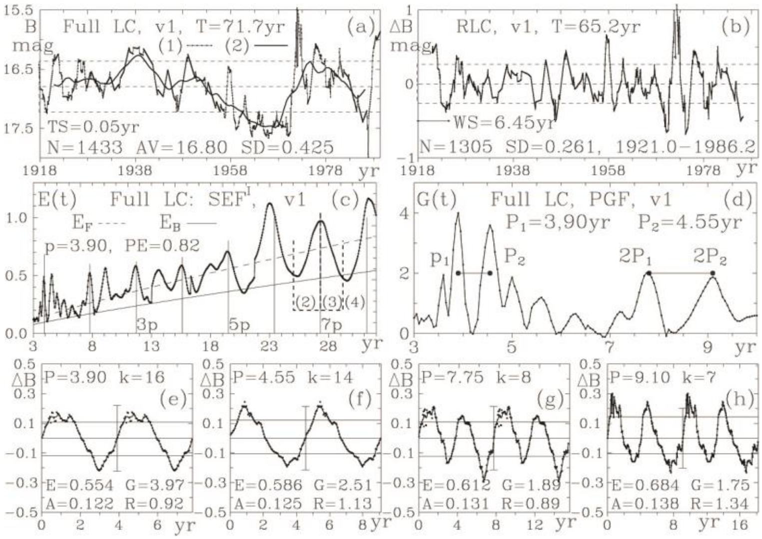

Fig. 3. SEF v1 analysis of Full LC. See the text.

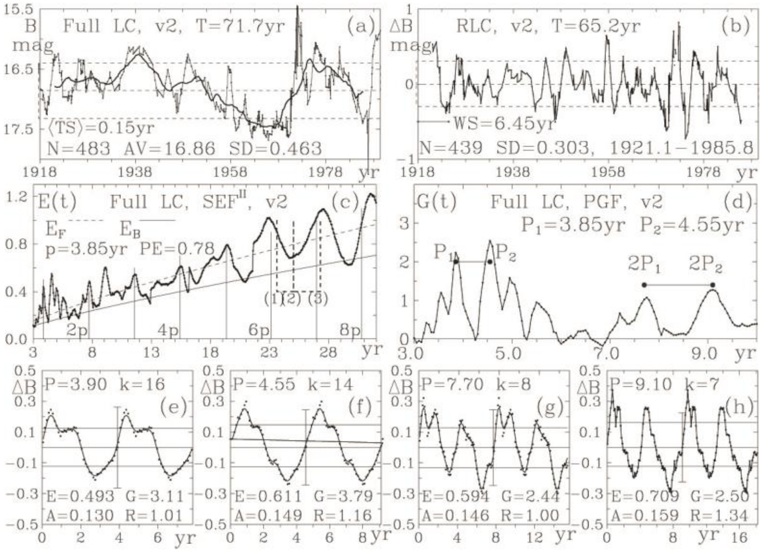

Fig. 4. SEF v2 analysis of Full LC. See the text.

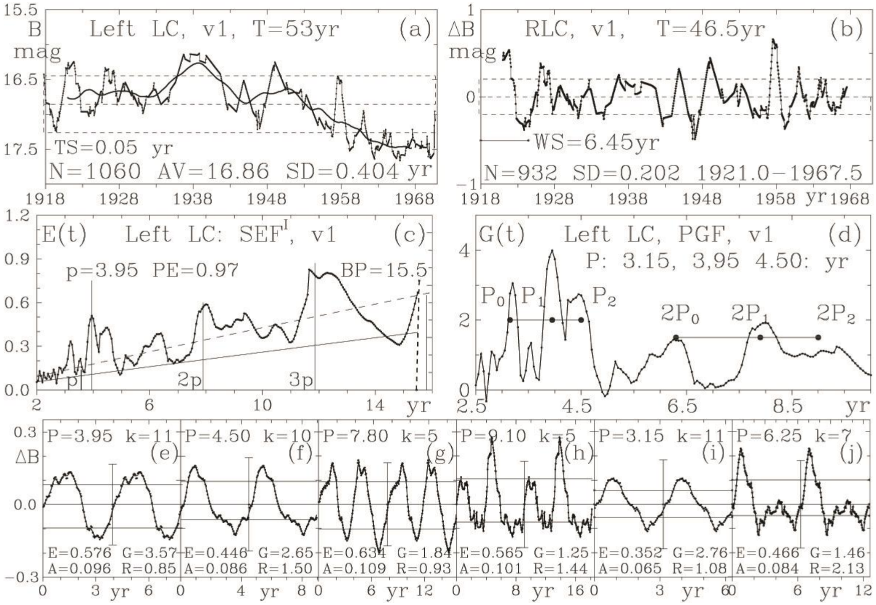

Fig. 5. SEF v1 analysis of Left LC. See the text.

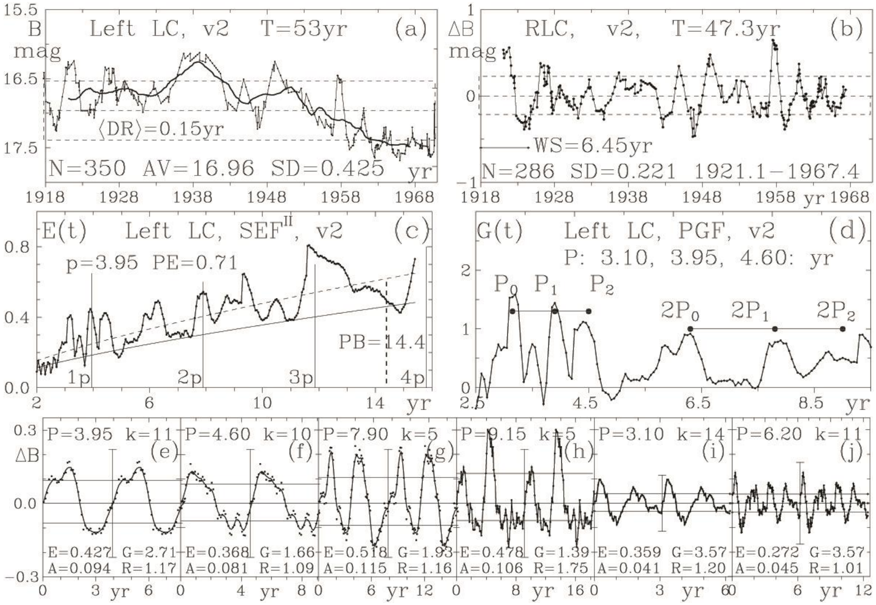

Fig. 6. SEF v2 analysis of Left LC. See the text.

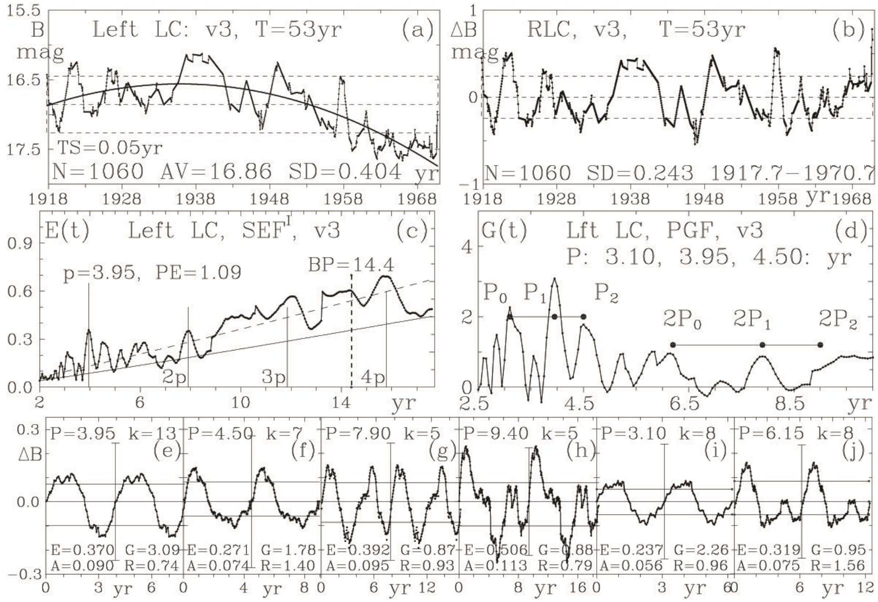

Fig. 7. SEF v3 analysis of Left LC. See the text.

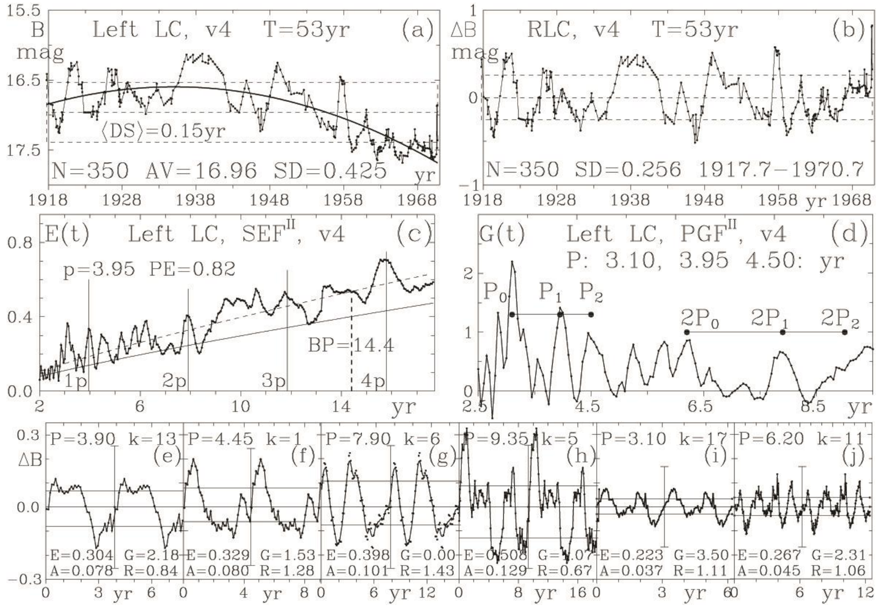

Fig. 8. SEF v4 analysis of Left LC. See the text.

In Figs. 3d–8d, the widths of the PGF humps of the large counterparts 2*p* are twice as large, but the relative hump width is again about 5%. However, the QP resolution is higher than the hump resolution. In Figs. 3d–8d, the prominent QPs are marked with dots. The QP value, measured by peak position or by the centre of the hump, varies within ± 1 dp or ± 0.05 yr. So, the QP error is 0.05 yr.

In Figs. 3d–8d, we reveal **3 prominent QPs.** The QPs at P_1 = 3.90 yr and P_2 = 4.55 yr are present everywhere. similar to the QP pair of Eta Car (4.9 and 5.6–5.7 yr) (G+25). Here, the QP 4.55 yr profile poses positive skewness, similar to the QP of 5.6–5.7 yr of Eta Car. AF And is known as a single LBV star, but the found QPs hint that it may be a binary LBV, as maintained by Gallagher et al. (1981). The orbital period should be about 4.5 yr. The QP at P_0 = 3.10 yr is absent in the Full LC (Figs. 3d–6d) but is clearly visible in the Left LC (Figs. 7d, 8d). We found additionally that the QP P_0 is variable and strongly prominent in 1940–1960 yr. For the present, the origin of the prominent QPs in AF And is unknown.

Two prominent QPs must have "**beat QPs"**. The beat period (BP) p_b from two periods p_1 and p_2 follows the formula $1/p_b = 1/p_1 - 1/p_2$ ($p_1 < p_2$). In Figs. 3c, 4c, the possible BPs are marked by triads of dashed vertical lines, (1), (2), (3). Four possibilities for p_1, p_2, and p_0 are considered. (1): 3.85, 4.60, 23.6; (2): 3.85, 4.55, 25.0; (3): 3.9, 4.55, 27.3; (4): 3.9, 4.5, 29.2. According to the QP values of P_1 and P_2 in Figs. 3d, 4d, the realistic cases are (3) and (2). So, the BPs, marked by the middle vertical lines, are 27.3 yr in Fig. 3c and 25.0 yr in Fig. 4c. The first BP coincides with $7P_1$. The second has a separate hump, but its prominence is weak. In Figs. 5c–8c, the BPs for the QPs P_0 and P_1 are marked by vertical dashed lines. They are close to the large counterparts $4P_1$. So, the beat periods are not remarkable.

3. SEF profiles of QP structures

Figs. 3(e–j)–8(e–j) show QP profiles, i. e., profiles of SEF structures, corresponding to the SEF peak values. For the visualisation, they are drawn twice. The profile may provide a hint about its reason, e.g., "obscure" or "flash". In spite of the nosed LC, different SEF variants produce similar profiles. The bottom panels in Figs. 3–8 show profiles a_j (here as ΔB) and their parameters. The dots represent raw profiles, and the curves show profiles that are smoothed through the AV of 5 neighbour points. *P* is the QP, i.e., the peak position in the PGF. *k* is the number of segments added for the profile. *E* and *G* are the peak values of SEF and PGF of the presented QP. *A* is the “one-side” AV of the profile *a*j. The vertical bar represents the AV SEF noise *D* of the profile. The ratio $R = A_1/|A_2|$, where A_1 and A_2 are AVs of the positive and negative parts of the profile, characterises the vertical asymmetry of the profile a_j. Positive *R* shows that the profile maximum (sometimes high and narrow) is more prominent than the profile minimum (sometimes shallow and wide) (see Figs. 3f–8f). Horizontal lines correspond to the A1, zero, and A2 levels.

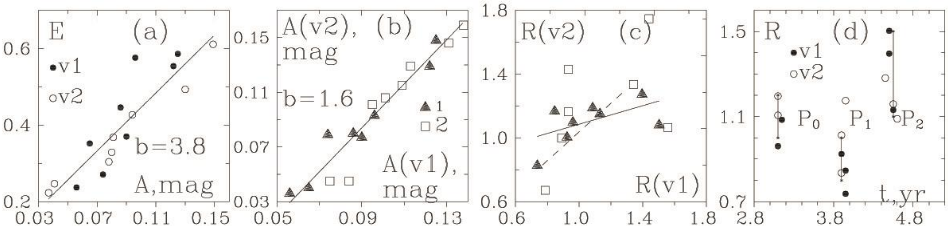

Fig. 9. Juxtaposition of profile parameters. See the text.

Fig. 9 juxtaposes parameters of QP profiles. The relevant linear fits with slope coefficients *b* are shown. In Figs. 9a, 9d, only data about the basic QPs (P_0, P_1, P_2), 8 dp from v1 (after resampling) and 8 dp from v2 (after completion) are used. In Fig. 9a, SEF values *E* are about 3.8 times higher than the average signal *A*. The reason is the division of the average signal *A* by the average noise *D*. In Fig. 9d, typical values of the ratio *R* for the QPs P_0, P_1, and P2 are about 1.1, 1.0, and 1.3, respectively. The vertical asymmetries in these profiles differ slightly. In Fig. 9b, the ratio of signals *A*(v2)/*A*(v1) for the basic QPs (1) and for 2*p* counterparts (2) is about1.6. The reason is that the resampling procedure in SEF v1 omits noise peaks and produces a slightly smoothed LC. In Fig. 9c, the ratios of the vertical asymmetry *R*(v2) and *R*(v1) for basic QPs (1) correlate faintly. Simultaneously, these ratios for 2*p* counterparts show no correlation. The reason is probably the physical and photometrical noise in the LC.

In this study, the P_2 profiles show positive skewness (Figs. 3f–8f). Similar positive skewness poses wholly different phenomena: LCs of RR Lyr, Delta Cep, and Mira Ceti, even the sale of the solar Wolf cycle. Therefore, we can speculate that P_2 is a display of some flashing, while P_1 may be a display of obscuration. Similar suspects hint at the QPs of Eta Car, $P_{1,}$ and P_2, respectively (G+25). Note also that the shapes of the odd and even components of the pairs of periods of 2*p* QPs (Figs. 3gh, 4gh, 5ghj–8ghj) are somewhat different. Such particularities of 2*p* are present in G+25. The reasons may be the noise in the LC.

4. Supplementary illustrations

Fig. 10 shows by large dots signal profiles a_j and by error bars noise profiles d_j. There *p*, *A* and *D* are the QP and AVs of the signal and noise, respectively. Small dots represent the used pair of raw profiles – from direct and reverse RLC processing (for 2 SEFs build). In (a), the small dots fall just on the positions of the resampled input LC. In (b) and (c), the small dot points have arbitrary positions, where the profile sampling causes additional profile smoothing. Depending on the beginning of the input LC, the pair of profiles has an arbitrary phase shift. The profiles in the bottom panels of Figs. 3–8 averaged (after phase shift) and drawn twice.

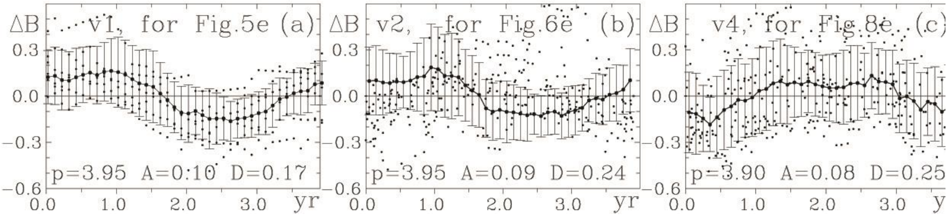

Fig. 10. Basic types of SEF profiles, corresponding to the SEF versions v1 (a), v3 (b), and v4 (c). See the text.

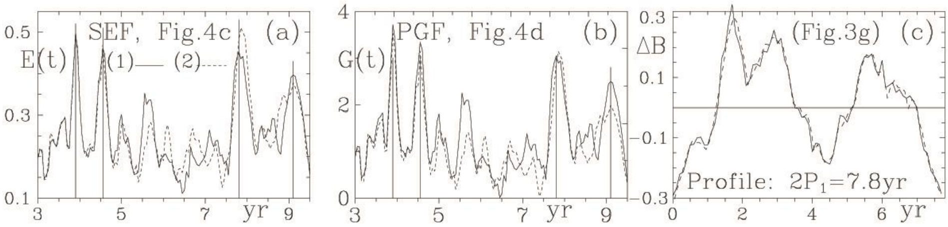

Fig. 11. Results from direct (1) or reverse (2) processing of RLCs: (a) – SEFs; (b) – PGFs; (c) – profiles. See the text.

Fig. 11 juxtaposes the PGFs from direct ((1), solid curves) or reverse ((2), dashed curves) processing of RLC. The differences between the curves are small. In all cases, the average SEFs, PGFs, and profiles are used, though.

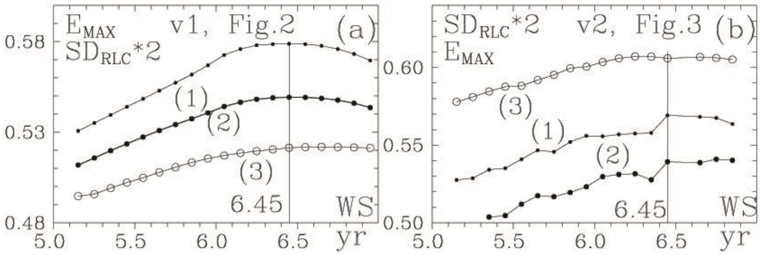

Fig. 12. Choice of optimal detrending WS = 6.45 yr for resampled (a) and completed (b) input LCs. See the text.

Fig. 12 shows the choice of WS according to the height of the PGF peak P_2 (1), AV of the three neighbouring points of the peak (2), and SD of the RLC after resampling (3) (v1, a) or completion (v2, b). The chosen WS of 6.45 yr corresponds to the beginning of the plateau of RLC SD (3).

5. Summary

We described and applied 4 variants of our SEF method for revealing quasi-periods in LCs. The method includes preliminary resampling or completing of the LC (if needed), as well as local or global flattening of the LC. Completing and global flattening seem preferable. The results are very close.

In the full LC of AF And we found a QP pair of 3.90 and 4.55 yr, similar to the QP pair of Eta Car (4.9 and 5.6–5.7 yr) (G+25). Here, the QP 4.55 yr profile poses positive skewness, similar to the QP of 5.6–5.7 yr of Eta Car. AF And is known as a single LBV star, but the found QPs hint that it may be a binary LBV, as maintained by Gallagher et al. (1981). The orbital period should be about 4.5 yr.

In the LC before 1972, we found a QP of 3.10 yr, strongly pronounced in 1940–1960. The QP of 3.1 yr seems unexplainable.

References

1. Gallagher, J. S., Kenyon, S. J,. Hege, E. K. (1981), Spectrophotometry of two luminous variable stars in the Andromeda galaxy. Astrophys. J. 249, 83
2. Gantchev, G., Valcheva, A., Nedialkov, P., Ovcharov, E. (2017), Structural Function Analysis of Selected Luminous Blue Variables in the Local Group, Bulg. Astron. J., 26, 16
3. Georgiev, Ts. (2023), Revealing of repeating structures in time series by the structure length eminence, Bulg. Astron. J. 38, 120 (G23)
4. Georgiev, Ts., Valcheva, A., Nedialkov, P., (2024), Photometric periods of M31LBV AF And identified via structure eminence function method, Publ. AO Belgrade (G+24)
5. Georgiev, Ts., Valcheva, A., Nedialkov, P., Stefanov, S., Moyseev, M., (2025), Periodicity in the light curve of Eta Car, Bulg. Astron. J., 43, 3 (G+25)
6. Humphreys, R. M., Weis, K., Davidson, K., Bomans, D. J., Burggraf, B., (2014), Luminous and Variable Stars in M31 and M33. II. Luminous Blue Variables, Candidate LBVs, Fe II Emission Line Stars, and Other Supergiants. Astrophys. J. 790 (1): 48
7. Joshi, Y.C., Sharma, K., Gangopadhyay, A., et al. (2019), A Long-term Photometric Variability and Spectroscopic Study of Luminous Blue Variable AF And in M31, Astron. J. 158 (5). 175
8. Szeifert, T., Humphreys, R. M., Davidson, K., Jones, T. J., Stahl, O., Wolf, B., Zickgraf, F. J., (1996), HST and groundbased observations of the `Hubble-Sandage' ariables in M 31 and M 33, Astron. Astrophys. 314: 131.

КВАЗИ-ПЕРИОДИ В КРИВАТА НА БЛЯСЪКА НА LBV ЗВЕЗДАТА AF ANDROMEDAE ИЗЯВЕНИ ЧРЕЗ МЕТОДА SEF

Ц. Георгиев, П. Недялков

Резюме

Ние анализираме историческа B-крива на блясъка на AF And (1918–1990) теставйки нашия метод на функцията на структурна изявеност (ФСИ, Structure Eminence Function, SEF). Методът извлича и характеризира повтарящи се структури (патерни), отговорни за квази-периоди (КПи) в редове от данни. ФСИ е зависимостта на размаха (амплитудата) на структурата от дължината на структурата. Позициите на максимумите на ФСИ индикират КПи. Предимство на метода е, че той представя профила на КП (формата на повтарящата се структура). Асиметрията на профила може да подскаже природата на КП, напр. “затъмняване” или “просветване”. В това изследване ние описваме и прилагаме 4 варианти на метода. Ние изтъкваме 2 КПи, от 3.90 и 4.55 год (± 0.05 год). Профилът на КП от 4.55 год има положителна асиметрия. В сравнение с Eta Car, у която в наша скорошна работа намерихме 2 видни КПи, максимумите на ФСИ у AF And са около 1.5 пъти по ниски. За сега ние не можем да свържем някой намерените КПи с установено периодично явление у AF And. Обаче, подобието на двойките КПи на Eta и Car AF And подсказва, че е възможно AF And е двойна система.